COMPUTATIONS OF COMPLEX FLOW CONFIGURATIONS USING A MODIFIED ELLIPTIC-BLENDING REYNOLDS-STRESS MODEL

S. Lardeau[1] *and R. Manceau*[2]

[1] *CD-adapco, 200 Shepherds Bush Road, London, W6 7NL, UK*
[2] *Departement of applied mathematics, Cagire group*
CNRS-University of Pau-INRIA, UMR 5142, 64013 Pau, France

sylvain.lardeau@cd-adapco.com

Abstract

Modifications of a low-Reynolds number Reynolds-stress model, based on the elliptic-blending approach of Manceau & Hanjalić (2002), are proposed. The main objective is to facilitate the use of Reynolds-stress approach in an industrial context. The new model is validated on canonical cases, such as channels and pipes and on a number of 3D attached and separated flows. Caveats of using Reynolds-Stress model are also emphasized, using a number of examples.

1 Introduction

In the past 40 years, RANS models, in particular eddy-viscosity models (EVMs), have been the workhorse in industry for computing turbulent flows, and they will remain the method of choice in the majority of cases in the foreseeable future. Transient methods, such as DES or hybrid RANS/LES, are still too time-consuming (set-up/meshing, computation, post-processing) to replace completely RANS models in industry as yet, for a number of reasons. In many cases, the level of accuracy provided by EVMs is sufficient. There is also a cost issue, associated not only with computational time, but also with the skills necessary to perform proper transient simulation, and extract the relevant information. There are of course very well known limitations to EVM, such as insensitivity to flow rotation or streamline curvature, poor performance in far-from-equilibrium conditions or for very anisotropic flows, or for intrinsically unsteady flows. Reynolds-stress models (RSM) seem to be the natural alternative to EVMs. However, they have been found, over the years, to be less reliable than EVMs when dealing with complex flow configurations, thus preventing their wider use in industry. The RSM proposed by Manceau & Hanjalić (2002), and referred to as EB-RSM in the following, is used as a basis to develop a more robust and industry-friendly RSM. The model is then tested on a number of canonical and complex flow configurations for which experimental and/or numerical data are publicly available.

Several modifications and additions to the original model and the subsequent formulation (Manceau, 2003; Dehoux *et al.*, 2012) are proposed to solve some of the known limitations of the RSMs: lack of numerical robustness, consistent performance and accuracy on non-perfect meshes. The goal is to provide a framework for the computation of complex flow configuration using RSMs. The first of the modifications proposed here deals with the near-wall formulation of the model, especially regarding the turbulent dissipation rate source term. The second important modification to the model is the addition of a new *all-*y^+ wall-treatment, based on that proposed for the elliptic-blending EVM of Billard & Laurence (2012). This modification is important in the context of industrial applications as it extends the use of the model to irregular meshes, and with near-wall resolution coarser than $y^+ \approx 1$. Further improvements are also presented. One point often cited in the literature but rarely addressed in the context of RSMs is the round-jet/plane-jet anomaly. The same approach as in the Standard $k-\omega$ model of Wilcox (2008) has been tested on free and rotating impinging jets. Effects of initial and boundary conditions is also discussed, as well as the pitfalls and limitations of the model.

2 Model formulation

The model derivation and the rational for using the elliptic-relaxation equation for a blending function can be found in Manceau & Hanjalić (2002), and is thus not repeated here. The model has gone through a number of small improvements over the years, and what we refer to as the *original model* is the one given in Dehoux *et al.* (2012). The transport equations for the

Reynolds-stresses $\overline{u_i u_j}$ are

$$\frac{D\overline{u_i u_j}}{Dt} = P_{ij} + \phi^*_{ij} - \varepsilon_{ij} + \mathcal{D}^t_{ij} + \frac{\partial}{\partial x_k}\left(\nu \frac{\partial \overline{u_i u_j}}{\partial x_k}\right) \quad (1)$$

where P_{ij} is the production tensor, ϕ^*_{ij} is the pressure-strain tensor, ε_{ij} is the dissipation-rate tensor and $\mathcal{D}^t_{ij}$ is the turbulent diffusion tensor. In the RSM framework, all terms but the production need to be modelled.

The following definitions are also used throughout the text

$$\begin{aligned} \mathcal{P} &= \frac{1}{2}P_{ii}; \qquad a_{ij} = \frac{\overline{u_i u_j}}{k} - \frac{2}{3}\delta_{ij} \\ S_{ij} &= \frac{1}{2}\left(\frac{\partial U_i}{\partial x_j} + \frac{\partial U_j}{\partial x_i}\right) \\ W_{ij} &= \frac{1}{2}\left(\frac{\partial U_i}{\partial x_j} - \frac{\partial U_j}{\partial x_i}\right) + \epsilon_{mji}\omega_m \end{aligned} \quad (2)$$

where $\mathcal{P}$ is the turbulent kinetic energy production, a_{ij} is the anisotropy tensor, ω_m is the system rotation vector, S_{ij} and W_{ij} being the strain-rate and rotation-rate tensor, respectively.

The EB-RSM is based on a *blending* of near-wall and weakly inhomogeneous models for the pressure-strain and dissipation

$$\phi^*_{ij} - \varepsilon_{ij} = (1-\alpha^3)(\phi^w_{ij} - \varepsilon^w_{ij}) + \alpha^3(\phi^h_{ij} - \varepsilon^h_{ij}) \quad (3)$$

where the blending parameter α is solution of the elliptic equation

$$\alpha - L^2\nabla^2\alpha = 1 \quad (4)$$

with the length-scale L defined as

$$L = C_l \max\left(\frac{k^{3/2}}{\varepsilon}, C_\eta \frac{\nu^{3/4}}{\varepsilon^{1/4}}\right) \quad (5)$$

An important property of this model is that is does not require the computation of an expensive wall distance. Indeed, the wall-normal direction can be computed directly from the elliptic-blending parameter, using

$$n_k = \frac{\partial\alpha/\partial x_k}{\sqrt{\frac{\partial\alpha}{\partial x_l}\frac{\partial\alpha}{\partial x_l}}} \quad (6)$$

In the outer region, the quasi-linear version of the SSG model Speziale *et al.* (1991) is used for the pressure-strain

$$\begin{aligned} \phi^h_{ij} &= -\left(C_1 + C^*_1\frac{\mathcal{P}}{\varepsilon}\right)\varepsilon a_{ij} \\ &\quad + \left(C_3 - C^*_3\sqrt{a_{kl}a_{kl}}\right)kS_{ij} \\ &\quad + C_4 k\left(a_{ik}S_{jk} + a_{jk}S_{ik} - \frac{2}{3}a_{lm}S_{lm}\delta_{ij}\right) \\ &\quad + C_5 k\left(a_{ik}W_{jk} + a_{jk}W_{ik}\right) \end{aligned} \quad (7)$$

and in the near-wall layer

$$\begin{aligned} \phi^w_{ij} &= -5\frac{\varepsilon}{k}\Big[\overline{u_i u_k}n_j n_k + \overline{u_j u_k}n_i n_k \\ &\quad - \frac{1}{2}\overline{u_k u_l}n_k n_l(n_i n_j + \delta_{ij})\Big] \end{aligned} \quad (8)$$

For the dissipation rate tensor, we use

$$\varepsilon^w_{ij} = \frac{\overline{u_i u_j}}{k}\varepsilon; \qquad \varepsilon^h_{ij} = \frac{2}{3}\varepsilon\delta_{ij} \quad (9)$$

where ε is solution of

$$\frac{D\varepsilon}{Dt} = \frac{1}{\tau}\left(C_{\varepsilon_1}\mathcal{P} - C_{\varepsilon_2}\varepsilon\right) + E + \mathcal{D}^t_\varepsilon + \frac{\partial}{\partial x_k}\left(\nu\frac{\partial\varepsilon}{\partial x_k}\right) \quad (10)$$

Here, we revert back to the original formulation proposed by Manceau & Hanjalić (2002). It was recently shown that the additional term E is instrumental in the good performance of the B-EVM in the near-wall region, although the original formulation of this term is slightly modified, following the developments of the B-EVM (Billard & Laurence, 2012), and restricted to the near-wall region

$$E = A_1\nu\overline{u_k u_l}n_k n_l\frac{k}{\varepsilon}\left(1-\alpha^3\right)\left(\frac{\partial||S_{ij}n_i||n_k}{\partial x_k}\right)^2 \quad (11)$$

The constant A_1 is calibrated by reference to channel flow for a large range of Reynolds numbers. The turbulent time-scale τ is simply defined as

$$\tau = \max\left(\frac{k}{\varepsilon}, C_t\sqrt{\frac{\nu}{\varepsilon}}\right); \quad (12)$$

C_{ε_1}	C_{ε_2}	C_s	σ_k	σ_ε	A_1	C_t
1.44	1.83	0.21	1.0	1.15	0.085	6
C_l	C_η	C_1	C^*_1	C_3	C^*_3	C_4	C_5
0.133	80	1.7	0.9	0.8	0.65	0.625	0.2

Table 1: Model constants for the EB-RSM.

For the computation of the turbulent diffusion terms in Eqs. (1) and (10) ($\mathcal{D}^t_{ij}$ and $\mathcal{D}^t_\varepsilon$), unlike in the original model, which was based on the Generalized Gradient Diffusion Hypothesis, we use a more robust Simple Gradient Diffusion Hypothesis where the turbulent eddy-viscosity ν_t is defined as

$$\nu_t = \left[(1-\alpha^3)\overline{u_i u_j}n_i n_j + \alpha^3 k\right]C_\mu\tau \quad (13)$$

The first part of the RHS yields the correct near-wall asymptotic behaviour, similarly to the B-EVM formulation. The second part is introduced to avoid unwanted oscillations away from walls, in regions where the gradient of α is not really well-defined. The constant C_μ is equal to 0.07.

For all the cases presented in the paper, the RSM results are compared with those obtained using two of

the most popular EVMs: the realizable $k-\varepsilon$ model (Shih *et al.*, 1995), combined in the present case with a two-layer wall-function, and the SST $k-\omega$ model (Menter, 1994, including the most recent improvements by the same author). Those two models are considered to represent the best compromise in terms of robustness and accuracy, and they are thus the models of choice for many industrial codes. An additional correction was added to the two eddy-viscosity models, namely a curvature correction (CC). The aim is to make the models more sensitive to curvature and rotational effects. For the SST $k-\omega$ model, the modification proposed by Smirnov & Menter (2009) was used. For the realizable $k-\varepsilon$, the model was adapted from the model of Arolla & Durbin (2013). For the former, the production term in both k and ω equation are multiplied by a function $f_{\rm rot}$, defined as

$$f_{\rm rot} = (1+C_{r_1})\frac{2r^*}{1+r^*}\left[1-C_{r_3}\tan^{-1}(C_{r_2}\tilde{r}\right] - C_{r_1} \tag{14}$$

where C_{r_1}, C_{r_2} and C_{r_3} are constants, and $r^* = S/\Omega$ is the strain-to-vorticity-rate ratio, defined in the absolute frame of reference. $\tilde{r}$ is function of the Lagrangian derivative of the strain-rate tensor DS_{ij}/Dt. For the second model (Arolla & Durbin, 2013), the eddy-viscosity coefficient C_μ of the realizable $k-\varepsilon$ model is directly modified to account for the same effect

$$C_\mu^* = \frac{C_\mu}{\alpha_1(|\eta_3|-\eta_3)+\sqrt{1-\alpha_2\eta_3}} \tag{15}$$

where $\eta_3 = \eta_1 - \eta_2$, $\eta_1 = \tau^2 S_{ij}S_{ij}$, $\eta_2 = \tau^2\Omega_{ij}^{mod}\Omega_{ij}^{mod}$. Ω_{ij}^{mod} is the modified rotation tensor, also function of the Lagrangian strain-rate derivative. Both models have been shown to improve significantly the results for the cases presented below, and are thus included here for a fairer comparison with the RSM.

Universal wall-treatment

For the near-wall treatment, the same strategy as in Billard & Laurence (2012) for the elliptic-blending EVM is adopted. The treatment of the dissipation equation is the same as that used in other low-Re EVM, and is thus not repeated here (Billard & Laurence, 2012). The only term requiring a specific treatment is the production of the Reynolds stresses P_{ij}. In the wall-oriented co-ordinate system (t,n), and under local equilibrium conditions, the ratio of the wall-normal component to the shear stress is equal to (Hadzić, 2001) $\overline{u_n^2}/\overline{u_t u_n} = -0.413/0.314$, which gives a shear-stress production equal to $P_{tn} = -1.315\mathcal{P}$. The turbulent kinetic energy production $\mathcal{P}$ is taken from Billard & Laurence (2012)

$$\mathcal{P} = 0.95\frac{\nu_t^+}{(1+\nu_t^+)^2} \tag{16}$$

with

$$\nu_t^+ = \kappa y^+\left[1-\exp\left(\frac{-y^+}{26}\right)\right]^2 \tag{17}$$

No other modification of the Reynolds-stress source terms was found to be necessary.

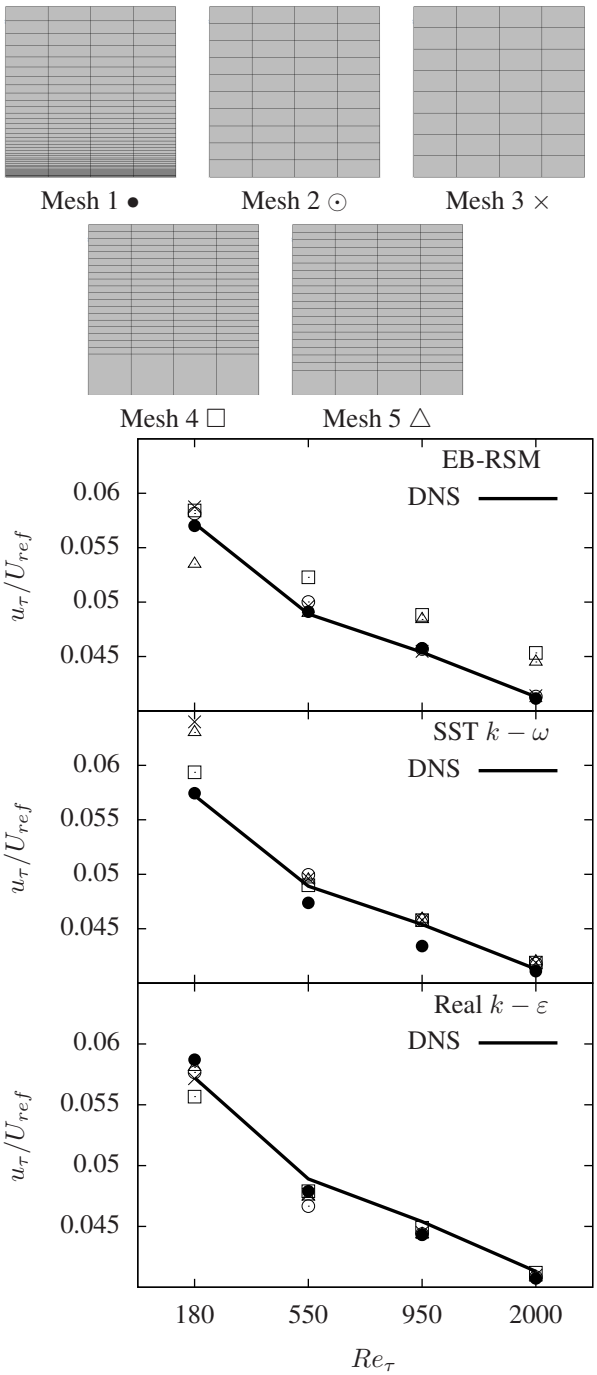

Figure 1: Evolution of wall friction velocity u_τ as a function of the Reynolds number for various mesh resolutions. Symbols are shown below the corresponding meshes.

Fig. 1 shows the evolution of the wall-shear stress u_τ as a function of the Reynolds number in channel flows for various mesh resolution (from $y^+ \approx 1$ with standard growth-rate to constant meshes with large first cell, and to variable growth rate, situation that is often found in practical applications). Results are compared with the DNS data of Hoyas & Jimenéz

(2008), for Reynolds number, based on the friction velocity, ranging from 180 to 2000. Both EVMs underestimate the wall-shear stress for the finest resolution (Mesh 1, •), while the EB-RSM is in good agreement with the DNS data across the range of Reynolds numbers computed. For the other mesh resolutions (Meshes 2-5), there is a small spreading in the computed u_τ, and this spreading seems to be more Reynolds-number dependent with the EVMs that with the EB-RSM. The relatively small spreading gives us confidence that the EB-RSM, associated with the new wall-function, will not be too sensitive to the mesh resolution in the near-wall region.

Round-jet/plane-jet anomaly and proposed correction

Following Pope (1978), the coefficient C_{ε_2} in the dissipation equation (Eq. 10) can be replaced by $C^*_{\varepsilon_2}$, defined as

$$C^*_{\varepsilon_2} = C_{\varepsilon_2} - \alpha^3 C_{\varepsilon_3} \chi \tag{18}$$

where χ is an invariant considered to be a measure of the vortex stretching

$$\chi = \tau^3 W_{ik} W_{kj} S_{ij} \tag{19}$$

However, this substitution was found to be rather unstable, as χ is allowed to vary from very low to very high values. A better method is to use a formulation akin to that proposed for the Standard $k-\omega$ model. In that case, the coefficient $C^*_{\varepsilon_2}$ is defined as

$$C^*_{\varepsilon_2} = C_{\varepsilon_2} \left[1 - \alpha^3 \left(1 - \frac{1 + 90|\chi|}{1 + 100|\chi|} \right) \right] \tag{20}$$

The coefficients in Eq. (20) were set to give the best results for a simple case of round and free jets (Fig. 2).

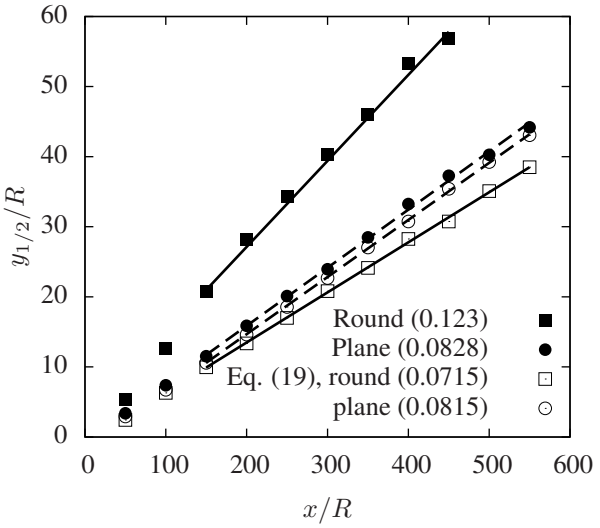

Figure 2: Streamwise evolution of a round jet and plane jet half-width, without and with correction (Eq. 20). The jet-spreading rates are given in the plots.

Initial condition

One of main issues faced when using many RANS models is the slow or non-convergence in the initial stage of the computation. This is particularly restrictive for low-Re model, and it has been attributed to a bifurcation property inherited from the low-Reynolds damping formulation. Rumsey *et al.* (2006) showed that alternative converged solutions could be obtained, depending on the initial and inflow conditions. To overcome the problem, a new method for generating initial conditions (Manceau, 2014) is used, which is user-independent, the only input to the method being a reference velocity $U_{\rm ref}$ that is usually the bulk velocity and can be computed from the inlet condition.

The method is divided into two steps. A first iteration is computed in order to obtain a sensible evaluation of the elliptic blending parameter α in the domain, as well as a mean velocity field that satisfies the main global constraint due to the geometry (flow rate, flow direction, boundary conditions). In order to do so, the turbulent variables are initialized so that the length scale L involved in the equation for α (Eq. 4) has the correct order of magnitude. This can be done by defining a friction velocity $u_\tau = 0.05\, U_{\rm ref}$, from which k and ε can be calculated, using

$$k = \frac{u_\tau^2}{\sqrt{C_\mu}}, \qquad \varepsilon = \frac{u_\tau^4}{\kappa \nu d^+_{\rm ref}} \tag{21}$$

with $\kappa = 0.41$, $C_\mu = 0.09$ and $d^+_{\rm ref} = 17$.

The second step of the method consists in re-initializing the flow field using the results $\alpha^{(1)}$ of the first iteration for α and $U^{(1)}$ for U to evaluate the distance to the wall and to provide the mean flow direction, respectively. α is bounded as $\alpha = \min(\alpha^{(1)}, 1 - 10^{-6})$ (in effect, saturating the distance to the wall at $y^+ = 235$), and a value of the normalized wall-distance d^+ is given by

$$d^+ = -d^+_{\rm ref} \ln(1 - \alpha) \tag{22}$$

The direction of the velocity field is preserved, but its amplitude is modified in order to impose a boundary layer profile

$$U_i = \min \left(1, \frac{U^+(d^+)}{||U^{pot}||} \right) U_i^{pot} \tag{23}$$

where $U^+(d^+)$ is given by Reichardt's law, and $U_i^{(1)}$ is the results of an inviscid soluion. The turbulent variables are then re-initialized using

$$\varepsilon = \frac{1}{\max\left(d^+_{\rm ref}, d^+\right)} \frac{u_\tau^4}{\kappa \nu}$$

and

$$k = \frac{\nu \varepsilon}{2 u_\tau^2} {d^+}^2 (1-\alpha)^{1/3} + \frac{u_\tau^2}{\sqrt{C_\mu}} \alpha^{1/3}.$$

The evolution of the normalized residuals for the simulation of a separated flow over a swept wing at

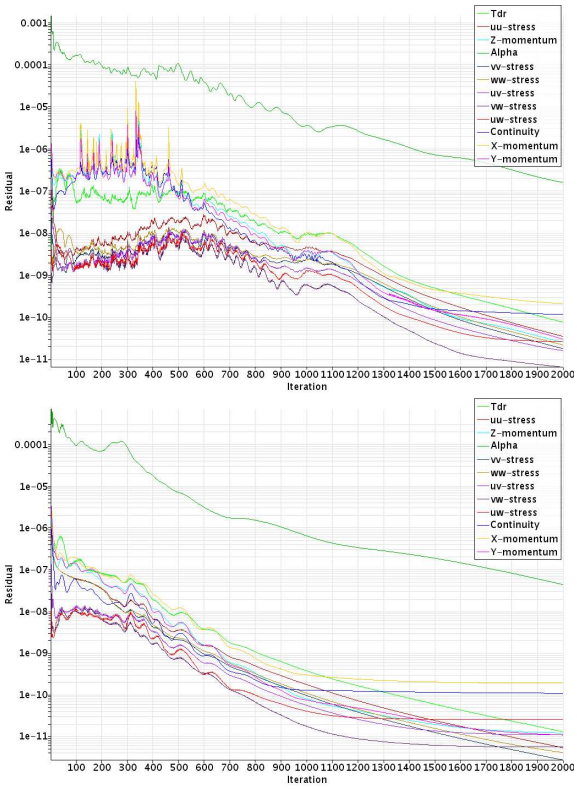

Figure 3: Convergence rate without (top) and with (bottom) new turbulence initialization, for the flow over a swept wing at high angle of attack (14°).

14° incidence is shown on Fig. 3. For both computations, the initial velocity field was first calculated using the inviscid solution, and for the second case, the above method was applied. For the same degree of convergence, the computational time was halved.

3 Results

For industrial practices, it is useful to distinguish between internal flows (e.g. pipe, channels, ...) and external flows (e.g. wings, cylinders, etc...). Elliptic-based models are known to perform better in the former category, provided that the mesh is regular enough, and the near-wall flow is well resolved. For external aerodynamics, flows are most of the time separated, the meshes are usually too coarse to properly resolve the near-wall physics, and this is why models such as the Spalart-Allmaras model or the Realizable $k-\varepsilon$ model are used, combined with a two-layer wall-treatment, effectively reducing the model to 1 transport equation in the viscous and buffer layers. For this reason, we are presenting results for both classes of flows, but focusing more on the second category, which is more challenging for the elliptic-based models.

Periodic curved pipe

A challenging flow has been recently computed by

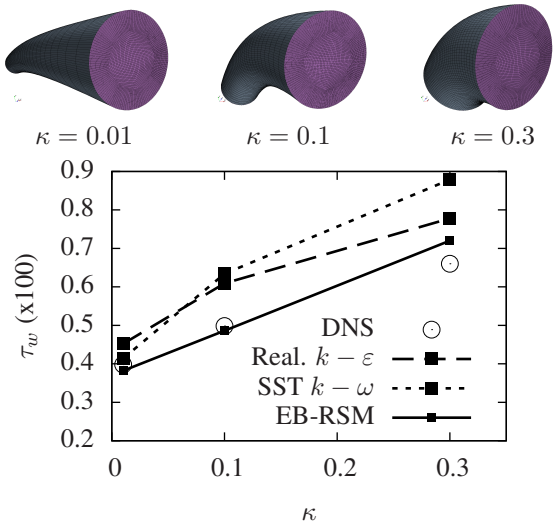

Figure 4: Evolution of averaged wall-shear stress in curved pipe flow (Noorani *et al*, 2013) as a function of the curvature parameter κ.

Noorani *et al* (2013), in a curved periodic pipe flow (Fig. 4), for three values (0.01, 0.1 and 0.3) of the curvature parameters $\kappa = R_a/R_c$, where R_a is the radius of the pipe cross-section and R_c is the radius of curvature of the pipe centerline. The Reynolds number, based on the pipe diameter and bulk velocity, is equal to 11,700. At this Reynolds number, the flow is expected to be fully turbulent for all but the highest value of κ. For all cases, the mass-flow rate across the periodic boundary is imposed, and the first point away from the wall is located around $y^+ \approx 1$.

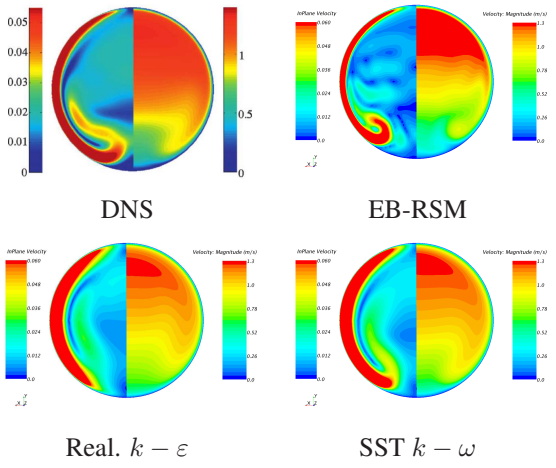

Figure 5: Contours of the in-plane (left half) and streamwise (right half) velocity, for the three different models compared to the DNS results of Noorani *et al* (2013), for $\kappa = 0.1$.

The spatially averaged wall-shear stresses τ_w are compared in Fig. 4. For $\kappa = 0.01$, the skin friction is

slightly overestimated by the two EVMs, and very satisfactory with the RSM, which is very similar to what is observed in channel flows. For $\kappa = 0.1$ and above, both EVMs tends to severely overestimate the wall-shear stress, while the EB-RSM remains in the same range as the DNS values. Note that for the highest value, the flow was found in DNS to intermittently relaminarize, lowering the space-time average value of τ_w, a feature impossible to capture with steady-state RANS.

Contours of the streamwise and in-plane velocity components are shown in Fig. 5. The EB-RSM is the only model able to capture accurately the secondary recirculation near the bottom axis of the flow, and the strong velocity asymmetry between the outside and inside part of the pipe.

Wing-tip vortex for NACA0012 at 10°

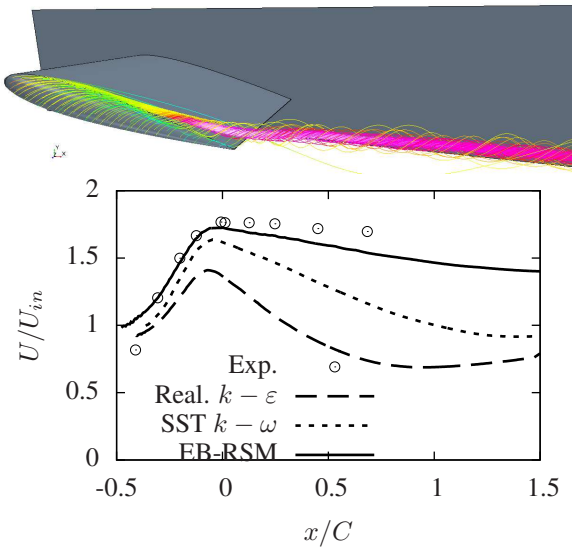

Figure 6: Flow configuration and streamwise velocity on the vortex centerline, of the NACA 0012 at 10° incidence (Chow *et al*, 1997).

The results of the computation of a trailing-edge vortex downstream of a NACA 0012 at 10° incidence (Chow *et al*, 1997) are shown on Figs. 6-7. The Reynolds number, based on the chord length C and the free-stream velocity is 4.6×10^6. A number of polyhedral meshes, with cell counts ranging from 250,000 to 7.7 million, were used for this study, but only results obtained with the finest mesh are shown here. A good measure of the performance of the model is the streamwise evolution of the wing-tip vortex centerline velocity (Fig. 6). The EB-RSM is the only model able to maintain the *solid body-like* rotation of the vortex up to the domain exit. The centerline velocity for both EVMs drops very quickly downstream of the trailing edge, and this drop was shown to be even faster without the CC. The results of the SST $k-\omega$ are consistent with those reported in Smirnov & Menter (2009), and illustrates the limit of such correction, compared to using a full RSM.

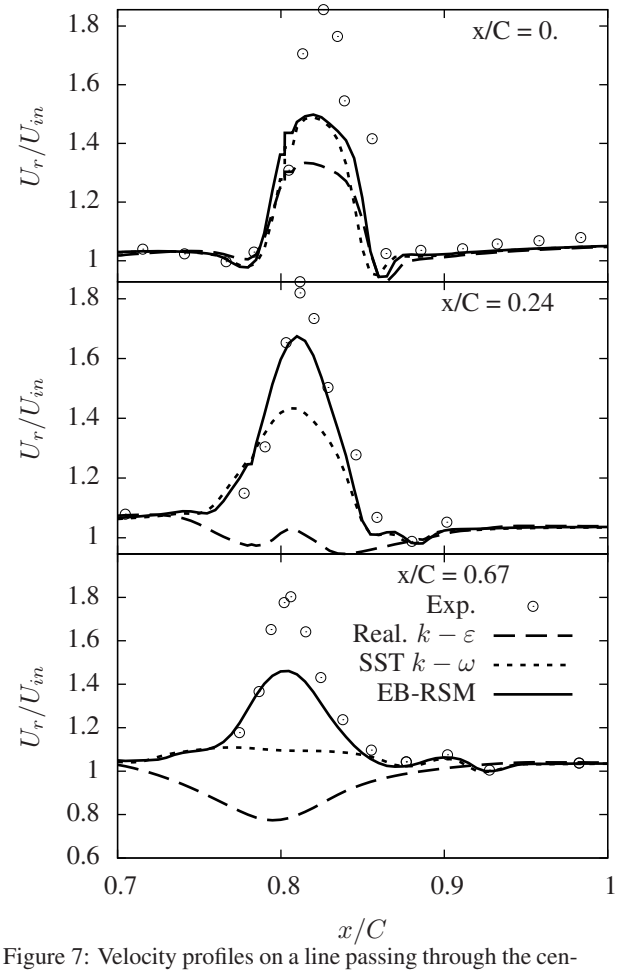

Figure 7: Velocity profiles on a line passing through the center of the vortex, at 3 different streamwise positions. Comparisons with the experiment of Chow *et al* (1997).

The axial velocity, at three different locations downstream of the trailing edge (located at $x/C = 0$), are shown in Fig. 7. The early vortex breakdown is also associated, in the case of EVMs, with a wider, more diffuse, velocity profile. For all three models, the results are nevertheless very much mesh dependent, and a minimum of 30 cells across the vortex core diameter (equal to twice the distance between the axial velocity peak and its minimum value) was necessary to avoid premature vortex breakdown.

Coanda Airfoil

The flow around a two-dimensional circulation airfoil was computed by Rumsey & Nishino (2011), using LES. The configuration (shown in Fig. 8, top) consists of a thick airfoil, with a small Coanda jet blowing on the upper part of the trailing edge. The jet height is $h/C = 0.0023$, and the radius of the Coanda surface is $r/C = 0.09463$. The Reynolds number based on the chord length and the free-stream velocity is equal to 490,000. Two different blowing ratio are re-

ported in Rumsey & Nishino (2011), but only the results obtained with the lowest ratio (equal to 0.1255) are given here. The domain was meshed using approximately 60,000 polyhedral cells, with 12 prism-layer in the near-wall region, where the resolution is such that $y^+ \approx 1$ over the surface of the airfoil. The plenum was also included in the computational domain.

Fig. 8 shows the velocity contours and streamlines around the Coanda section of the flow, and in the recirculation region. At first, the EB-RSM is the best at predicting the length and shape of the recirculation flow. The worst results are obtained with the SST model, with too long a recirculation bubble, consistent with results of Rumsey & Nishino (2011).

Model	C_L	θ_{sep}
LES	1.36	67°
EB-RSM	1.88	72 °
SST $k-\omega$	1.27	52°
Real. $k-\varepsilon$	1.61	70°

Table 2: Lift coefficient and angle of separation for the Coanda airfoil.

The performance of the model is quantified in Table 2 by comparing the lift coefficient and the jet separation angles (θ_{sep}). Surprisingly, C_L is significantly over-estimated with the EB-RSM, although the separation is close to the LES results. The origin of the discrepancy between the lift coefficients can be more clearly seen when comparing the evolution of the pressure coefficient around the bluff body in Fig. 9. Both the EB-RSM and the Realizable $k-\varepsilon$ (with curvature correction) tends to over-predict C_p on both sides. The large discrepancy around the leading edge on the suction side is linked to a very low turbulence activity in this region. This is similar to a *relaminarization* of the flow field due to combined effects of low-Re damping, time-scale limiter and favorable pressure gradient. The boundary layer is thus thinner when interacting with the Coanda jet, partly explaining the small difference in the separation point.

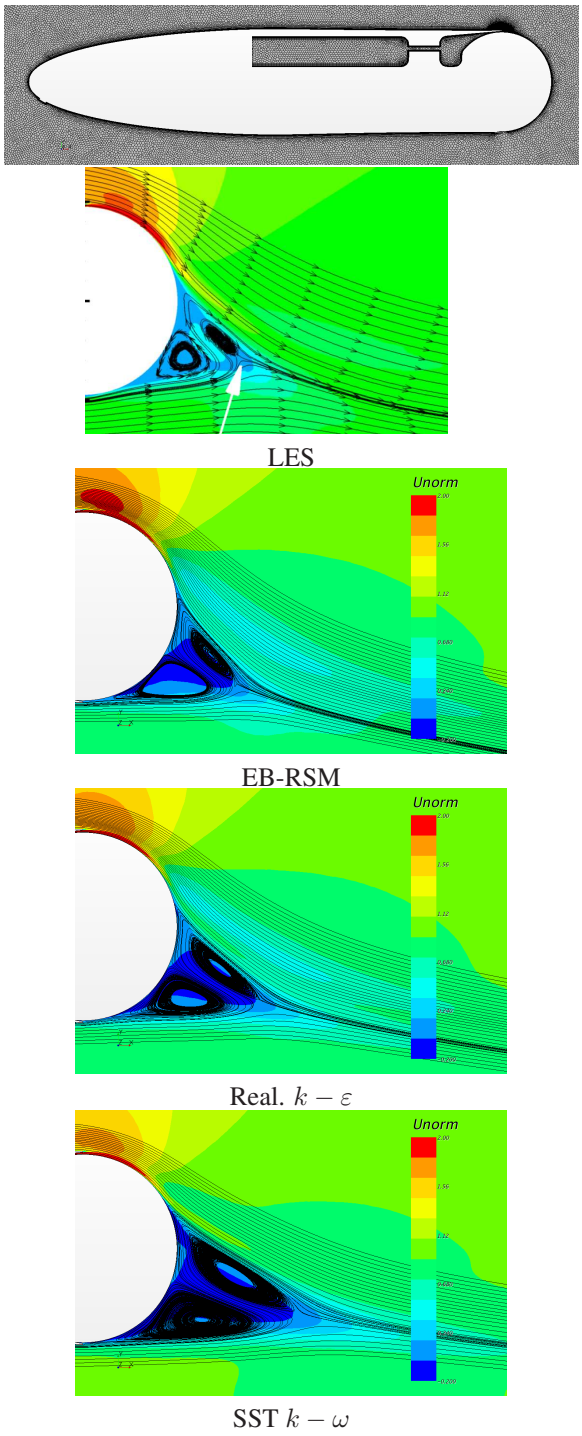

Figure 8: Velocity contours downstream of coanda airfoil at low injection Mach number ($M_j = 0.39$) (Rumsey and Nishino, 2001).

4 Conclusions

Several modifications of the EB-RSM of Manceau & Hanjalić (2002) have been proposed, in order to promote numerical robustness, implemented in a commercial code (STAR-CCM+) and tested on a number of canonical and complex flow configurations. The new model was compared with more established, simpler, two-equations eddy-viscosity based models.

Overall, the model outperforms the two EVMs, on all internal cases tested, and the results were obtained with comparable convergence rates, albeit at a slightly higher cost. For external aerodynamics, the results have been found to be more mixed, in line with previous studies. The model is more sensitive to the initial conditions, thus requiring the type of methodology developed by Manceau (2014), but also to the near-wall meshing, and to the flow resolution far away from walls. One of the main problem with the model is unwanted relaminarization, especially around bluff bodies. This was illustrated by Coanda airfoil (Rumsey and Nishino, 2011). For all cases, the mesh restriction was also slightly higher than for standard EVM, and

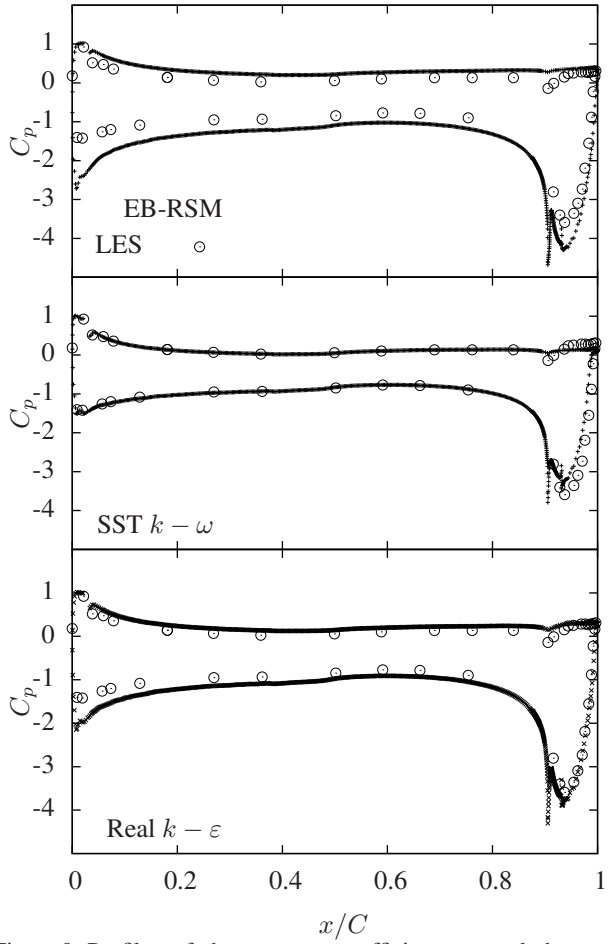

Figure 9: Profiles of the pressure coefficients around the coanda airfoil (Rumsey & Nishino, 2011).

the new initialization, introduced in the first section, was used for every computation, to reduce the computational cost, and avoid unwanted oscillations.

References

Arolla S.K. and Durbin P.A. (2013), Modeling rotation and curvature effects within scalar eddy-viscosity model framework. *Int. J. of Heat and Fluid Flow*, Vol. 39, pp 78–89.

Billard F. and Laurence D. (2012), A robust $k-\varepsilon-v^2/k$ elliptic blending turbulence model applied to near-wall, separated and buoyant flows. *Int. J. of Heat and Fluid Flow*, Vol. 33(1), pp. 45-58.

Chow J.S., Zilliac G.G. and Bradshaw P. (1997), Mean and turbulence measurements in the near field of a wingtip vortex. *AIAA J.*, Vol. 35(10), pp. 1561-1567.

Dehoux F., Lecocq Y., Benhamadouche S., Manceau R. and Brizzi L.-E. (2012) Algebraic modeling of the turbulent heat fluxes using the elliptic blending approach. Application to forced and mixed convection regimes. *Flow, Turbulence and Combustion*, Vol. 88, pp. 77-100.

Hoyas S. and Jiménez J. (2008), Reynolds number effects on the Reynolds-stress budgets in turbulent channels. *Physics of Fluids*, Vol. 20, pp. 101511.

Manceau R. and Hanjalić K. (2002), Elliptic blending model: A new near-wall Reynolds-stress turbulence closure. *Physics of Fluids*, Vol. 14, pp. 744.

Manceau, R. (2003), Accounting for wall-induced Reynolds stress anisotropy in Explicit Algebraic Stress Models. In: Proc. 3rd Symp. Turb. Shear Flow Phenomena, Sendai, Japan.

Manceau R. (2014), "A two-step automatic initialization procedure for RANS computations", in preparation.

Menter F.R. (1994), Two-equation eddy-viscosity turbulence models for engineering applications. *AIAA J.*, Vol. 32(8), pp. 1598-1605.

Noorani A., El Khoury G.K. and Schlatter P. (2013), Evolution of turbulence characteristics from straight to curved pipes. *Int. J. of Heat and Fluid Flow*, Vol. 41, pp. 16-26.

Pope S. (1978), An explanation of the turbulent round-jet/plane-jet anomaly. *AIAA J.*, Vol. 16(3), pp. 279-281.

Rumsey, C.L., and Nishino, T. (2011), Numerical study comparing RANS and LES approaches on a circulation control airfoil. *Int. J. Heat and Fluid Flow* Vol. 32(5), pp 847–864.

Rumsey, C.L., Pettersson Reif, B.A. and Gatski, T.B. (2006), Arbitrary steady- state solutions with the KEpsilon model. *AIAA J.*, Vol. 44(7), pp. 1586–1592.

Shih T.-H., Liou W.W., Shabbir A., Yang Z. and Zhu J. (1995), A new $k-\varepsilon$ eddy viscosity model for high Reynolds number turbulent flows. *Computers & Fluids*, Vol. 24(3), pp. 227-238.

Speziale C., Sarkar S. and Gatski T. (1991), Modelling the pressurestrain correlation of turbulence: an invariant dynamical systems approach. *J. Fluid Mech.*, Vol. 227, pp. 245-272.

Smirnov P.E. and Menter F.R. (2009), Sensitization of the SST turbulence model to rotation and curvature by applying the Spalart-Shur correction term. *J. of Turbomachinery*, Vol. 131, pp. 041010.

Wilcox D.C. (2008), Formulation of the $k-\omega$ turbulence model revisited. *AIAA J.*, Vol. 46(11), pp. 2823-2838.